Available online at www.sciencedirect.com
SCIENCE DIRECT®
Polymer 44 (2003) 5869–5876
polymer
www.elsevier.com/locate/polymer

Orientation and structure development in melt-spun Nylon-6 fibres

J.P. Penning[a,*], J. van Ruiten[a], R. Brouwer[a], W. Gabriëlse[b]

[a]*Centre for Fibre Technology, DSM Fibre Intermediates, P.O. Box 18, NL-6160 MD Geleen, The Netherlands*
[b]*Department of Research and Technology, DSM Engineering Plastics, P.O. Box 604, NL-6160 AP Geleen, The Netherlands*

Received 14 January 2003; received in revised form 6 May 2003; accepted 6 May 2003

Dedicated to Prof. Ian M. Ward on the occasion of his 75th birthday

Abstract

A network model is applied to describe the deformation behaviour of melt-spun Nylon-6 fibres obtained at different spinning and drawing conditions. The network draw ratio is determined from analysis of true stress–strain curves and correlated with fibre orientation. From this analysis it appears that the deformation behaviour of Nylon-6 fibres adheres to a pseudo-affine mechanism. The results are discussed in terms of the semicrystalline nature of Nylon-6 fibres. By means of on-line birefringence measurements, wide angle X-ray scattering (WAXS) and solid-state NMR, it is shown that the crystalline and amorphous phases in Nylon-6 respond in a different way to network deformation. In the spin line, an affine (rubber-like) deformation mechanism is observed and this rubber-like network behaviour is transferred to the amorphous phase. After winding and conditioning of the spun fibres, a crystalline phase with relatively high orientation is formed which deforms according to a pseudo-affine mechanism upon further stretching.
© 2003 Elsevier Ltd. All rights reserved.

Keywords: Nylon-6 fibres; Network deformation model; Structure characterization

1. Introduction

Synthetic fibres from semicrystalline polymers such as polyamides and polyesters find use in a variety of applications ranging from textiles to reinforcement of car tires. For successful use in these applications, it is necessary to obtain oriented fibre structures in order to realize sufficiently high tenacities and to remove the large irreversible deformation inherent to unoriented flexible polymers. The most common process for producing synthetic fibres is melt spinning, where partial molecular orientation is achieved by drawing down the spinning thread using high wind-up speeds. In spite of technological developments that have made it possible to achieve very high wind-up speeds up to 10 km/min, it has not been possible to achieve fully oriented structures by means of spinning alone. Therefore, additional hot-drawing of the spun fibre is often required in order to achieve the desired balance of fibre properties (e.g. modulus, tenacity, elongation). The processing steps of spinning and subsequent drawing are strongly interrelated in the sense that drawability and maximum attainable properties depend to a large extent on wind-up speed and the orientation achieved during spinning.

The development of molecular orientation and mechanical properties in the separate stages of spinning and drawing may be interpreted in terms of a network deformation model. The elementary ideas of rubber-like network deformation in melt-spun polymer fibres have been pioneered by Ward and co-workers [1,2] already in the 1960's. Their early work on polyethylene terephthalate (PET) revealed the existence of a molecular network, behaving according to the theory of rubber elasticity, in the melt-spun fibres. The concept of a molecular network being present in spun fibres has led to the idea that subsequent processing steps (such as hot-drawing) simply amount to a further deformation of the initial network developed during spinning. The network approach allows to compare the orientation and properties of yarns obtained by different process routes on the basis of a single parameter, being the network draw ratio (NDR). A crucial assumption is that the network retains its initial topology throughout the various processing steps.

The network deformation concept has been applied

* Corresponding author. Tel.: +31-46-476-0277; fax: +31-46-476-1298.
E-mail address: janpaul.penning@dsm.com (J.P. Penning).

0032-3861/03/$ - see front matter © 2003 Elsevier Ltd. All rights reserved.
doi:10.1016/S0032-3861(03)00535-4

successfully to describe the orientation and mechanical behaviour of PET fibres [3–6]. However, very few studies have addressed this issue for other polymers such as polyamides, although they are commercially as well as technically important fibre polymers. In a recent study [7], the network deformation concept has been applied to describe the drawability of melt-spun Nylon-4.6 fibres (Stanyl® from DSM).

In the present study, the applicability of the network deformation model is examined for Nylon-6 fibres obtained by different spinning and drawing processes. In a first approach, the NDR of different Nylon-6 fibres is determined from the superposition of true stress–strain curves [3–7] and compared to the overall orientation determined from birefringence measurements. In the second part of this paper, the semicrystalline nature of Nylon-6 is addressed. On-line birefringence measurement, wide angle X-ray scattering (WAXS) and solid-state NMR techniques have been used to study the orientation behaviour of the amorphous and crystalline phases separately. The development of orientation in the two phases is interpreted in terms of known models for network deformation.

2. Experimental

2.1. Sample preparation

Nylon-6 multi-filament yarns were produced on lab-scale spinning equipment, consisting of a 25 mm single-screw extruder, an electrically heated melt transporting line equipped with metering pumps, and a spinneret having 24 circular spinning holes. Pre-dried Nylon-6 granulate is melted and extruded through the spinneret plate, and the extruded multi-filament yarn is subsequently cooled and wound at take-up speeds ranging from 500 to 6500 m/min. After winding and conditioning, the spun yarns are hot-drawn in two stages using an Erdmann Drawmod drawing frame consisting of four heated godets. The applied draw ratios are in the range from 2.0 to 4.5 and the drawing temperature in the first and second drawing stage is 140 and 185 °C, respectively.

Two different Nylon-6 spinning grades were used. A high molecular weight Nylon-6 grade, having a relative viscosity of 2.85 (as determined at 20 °C at 1.0 wt% in H_2SO_4), corresponding to a molecular weight of $M_n = 21\,500$ g/mol, was used for spinning at winding speeds up to 2000 m/min. A lower molecular weight grade, having a relative viscosity of 2.45, corresponding to a molecular weight of $M_n = 16\,400$ g/mol, was used for spinning at winding speeds higher than 3000 m/min.

2.2. Mechanical characterization

Fibre mechanical properties have been determined using Zwick 1435 and Textechno Statimat tensile testers. Testing conditions are in accordance with the BISFA Testing Methods for Polyamide Filament Yarns (Edition 1995). In agreement with the BISFA method, gauge length (GL) and crosshead speed (CHS) are chosen GL = 500 mm and CHS = 500 mm/min for yarns having an elongation at break lower than 50%, and GL = 250 mm and CHS = 1000 mm/min for yarns having an elongation at break higher than 50%. The nominal stress σ_{nom} (expressed in cN/dtex) is determined from the force divided by the linear density of the undeformed sample. The true stress is determined from $\sigma_{true} = \sigma_{nom} \times \lambda_{tens}$. Here, λ_{tens} is the conventional tensile strain, $\lambda_{tens} = L/L_{0,}$ where L and L_0 represent the deformed and undeformed sample lengths, respectively. The NDR of the fibre is determined by shifting the tensile data along the strain axis to match the curve of an unoriented reference yarn, according to the method described by Long and Ward [4]. The shift is accomplished by multiplying the tensile strain λ_{tens} with a factor λ_{shift}. NDR, that represents the total deformation of the molecular network imposed during spinning and drawing, then corresponds with λ_{shift} needed to obtain a match between the tensile data of sample and reference yarn. The 'true strain' λ_{true} of the sample is the sum of all deformations imposed during spinning, drawing and tensile testing and corresponds to $\lambda_{true} = \lambda_{tens} \times$ NDR. Finally, the 'true stress - true strain' curve, or simply 'true stress–strain' curve is represented by $\sigma_{nom} \times \lambda_{true} = \sigma_{true} \times$ NDR as a function of λ_{true}. It should be noted that a stress level of 1.0 cN/dtex corresponds to about 114 MPa for Nylon-6 fibres.

2.3. Structure characterization

For a selected number of fibres in this study, fibre structure (crystallinity, orientation and phase composition) has been characterized using different methods.

Crystalline orientation has been determined by means of wide-angle X-ray scattering (WAXS), from the azimuthal scan of the α 0.14.0 meridional reflection located at $2\theta = 77.5°$. The Hermans orientation factor f_c was calculated from the integrated peak intensities as a function of azimuthal angle φ. It is noted that the tail of the neighbouring γ-reflection (at $2\theta = 79°$) contributes to the total peak intensity. Hence, the value for f_c obtained by this procedure is heavily weighted towards the orientation of the α-crystals but may contain some contribution from the crystalline γ-phase (if present).

The orientation factors of the amorphous and crystalline phases have also been determined by means of ^{13}C solid-state NMR using a two-dimensional rotor-synchronized magic-angle spinning (MAS) experiment, described in detail elsewhere [8]. By using a ^{13}C relaxation time filter, the orientation in the rigid and mobile regions can be determined separately. The rigid and mobile phases are associated with the crystalline and amorphous phases in the fibre structure. However, it is important to note that there need not be an exact correspondence between the

'NMR-rigid' phase and the 'WAXS-crystalline' phase. The NMR-rigid phase may contain constrained amorphous material of low molecular mobility having a lower orientation than the crystals. In practice, the orientation factor of the NMR-rigid phase turns out to be somewhat lower than that of the WAXS-crystalline phase, supporting this idea.

The relative amounts of α- and γ-crystals have been determined by ^{13}C CPMAS spectroscopy. From high-resolution ^{13}C spectra, the α- and γ-crystalline phases can be distinguished for the reason that some methylene carbons have a chemical shift that is sensitive to crystalline modification. A ^{13}C T_1 relaxation time filter is used to suppress the amorphous methylene signals. The experiment is described in detail in Ref. [8].

The volume fraction of crystallinity V_c is calculated from the sample density ρ, determined using a CCl_4/*n*-heptane gradient column, on the basis of the formula

$$V_c = (\rho - \rho_a)/(\rho_c - \rho_a) \quad (1)$$

where ρ_a and ρ_c are the densities of the amorphous and crystalline phases, respectively. In the present work, the density of the amorphous phase is assumed to have a constant value of $\rho_a = 1090\ kg/m^3$ [9,10], independent of amorphous orientation. For Nylon-6, the density of the crystalline phase may be written as

$$\rho_c = \varphi_\alpha \rho_{c,\alpha} + \varphi_\gamma \rho_{c,\gamma} \quad (2)$$

where φ_α and φ_γ are the relative amounts of α- and γ-crystals as determined from ^{13}C solid-state NMR ($\varphi_\alpha + \varphi_\gamma = 1$) and $\rho_{c,\alpha}$ and $\rho_{c,\gamma}$ are the densities of the α- and γ-crystalline phases, respectively. For the present series of samples, the crystalline density of the α- and γ-phases has been determined from the unit cell parameters obtained from WAXS peak positions. Within the investigated range, the crystalline densities appeared to change little with processing conditions, and therefore averaged values of $\rho_{c,\alpha} = 1180\ kg/m^3$ and $\rho_{c,\gamma} = 1150\ kg/m^3$ have been used. The values are in good agreement with experimental data obtained by others, but are lower than the theoretical maximum values of $\rho_{c,\alpha} = 1230\ kg/m^3$ and $\rho_{c,\gamma} = 1190\ kg/m^3$ [11].

When crystallinity and crystalline orientation are known, the amorphous orientation factor f_a can be obtained by subtracting the crystalline orientation from the overall orientation as determined from birefringence. This is done on the basis of the well-known equation given by Stein and Norris [12]

$$f_a = \frac{\Delta n - V_c f_c \Delta n_c^0}{(1 - V_c)\Delta n_a^0} \quad (3)$$

where Δn is the sample birefringence and Δn_c^0 and Δn_a^0 represent the intrinsic birefringence of the crystalline and amorphous phases, respectively. The sample birefringence was determined using a Zeiss polarizing microscope equipped with a Quartz compensator. The intrinsic birefringence values for the crystalline and amorphous phases were assumed to be $\Delta n_c^0 = 0.089$ and $\Delta n_a^0 = 0.078$, based on literature data [9].

2.4. On-line measurement of birefringence during spinning experiments

The fibre orientation in the spinning yarn bundle has been determined by means of on-line birefringence measurement. A measuring device, developed by Acordis Industrial Fibres Research, has been used to this end. The measurement technique is based on the phase retardation of a polarized laser beam passing through the spinning filaments. A detailed description of the apparatus and the underlying principle of measurement can be found in Ref. [13]. An example of this type of apparatus is described by Nagasawa et al. [14] in a study on stress relaxations in glassy polymers. In the present spinning experiments, the measurements have been carried out at a position below the solidification point of the spin line where the filaments have reached their final speed, diameter and spin line orientation.

3. Results and discussion

In this study, a series of Nylon-6 yarns with different processing history has been obtained by spinning at various wind-up speeds and subsequent hot-drawing. In line with common fibre nomenclature we refer to the different samples as LOY (Low Oriented Yarn, spun at wind-up speeds <2000 m/min), POY (Partially Oriented Yarn, spun at wind-up speeds >3000 m/min) and FDY (Fully Drawn Yarn, i.e. yarns obtained after hot-drawing).

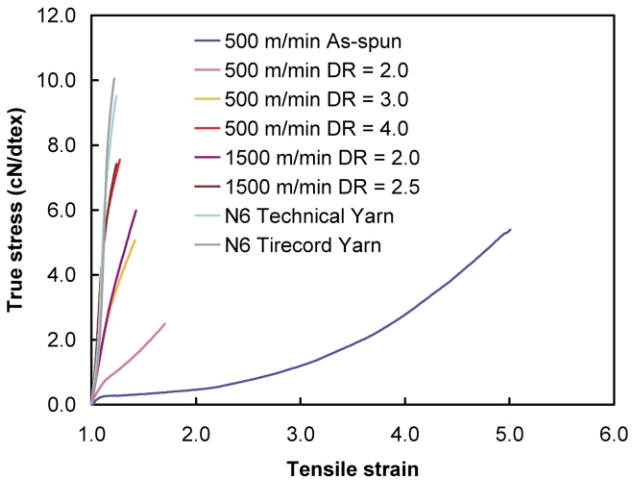

Fig. 1. True stress as a function of tensile strain (L/L_0) for Nylon-6 yarns obtained at different wind-up speed and draw ratio, as indicated in the legend. A commercially available Nylon-6 technical and tyre cord yarn are also included in this graph.

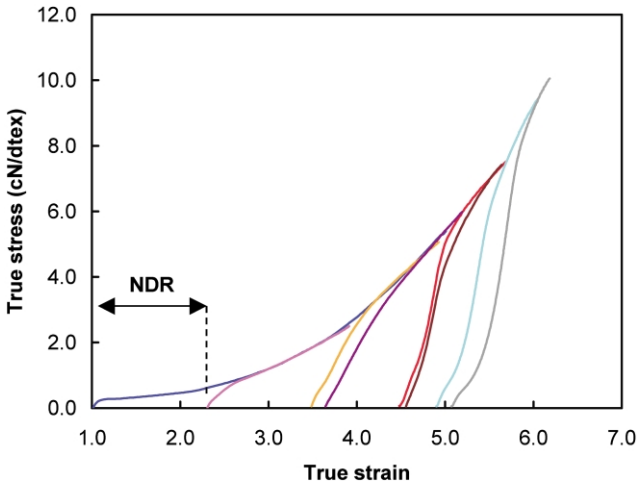

Fig. 2. True stress–strain curves for the Nylon-6 yarns from Fig. 1, shifted horizontally to form a continuous mastercurve. The network draw ratio (NDR) for a given yarn is obtained from the starting point of the shifted true stress–strain curve, as indicated by the arrow.

3.1. Evaluation of the network draw ratio

Fig. 1 shows true stress as a function of conventional tensile strain for a series of LOY (spun at 500–1500 m/min) and the FDY drawn from these. In Fig. 2, the curves have been shifted horizontally (along the strain axis) in such a way that the final portion of the shifted curve coincides with the 500 m/min LOY reference curve. The shift is accomplished by multiplying the tensile strain data with a factor λ_{shift}. The value of λ_{shift} needed to obtain a match between the tensile curves of sample and reference yarn corresponds to the NDR, that represents the total deformation of the molecular network imposed during spinning and drawing [4]. The value of NDR corresponds to the starting point of the shifted curve, and as such NDR can be read directly from the true stress–strain curve, as is shown in Fig. 2 for the 500 m/min yarn with DR = 2.0 yarn. The value of NDR obtained in this way is of course relative to the 500 m/min LOY reference. Based on extrapolation of birefringence data, as described in Ref. [7], it was found that the LOY precursor itself has a small network deformation, corresponding to NDR = 1.24.

It is seen in Fig. 2 that the shifted true stress–strain curves give an excellent fit to form a continuous mastercurve. This is indicative of a constant network topology for this set of yarns with different wind-up speed and drawing history.

Fig. 3 shows a series of true stress–strain curves for undrawn yarns obtained over a wide range of wind-up speeds (500–6500 m/min), that have been shifted horizontally coincide with the 500 m/min LOY curve. For yarns spun at wind-up speeds below 4000 m/min, a good fit with the mastercurve is obtained. For yarns spun at wind-up speeds above 4000 m/min, on the other hand, the shifted true stress–strain curves coincide with the mastercurve only in the final strain-hardening regime. This result indicates a

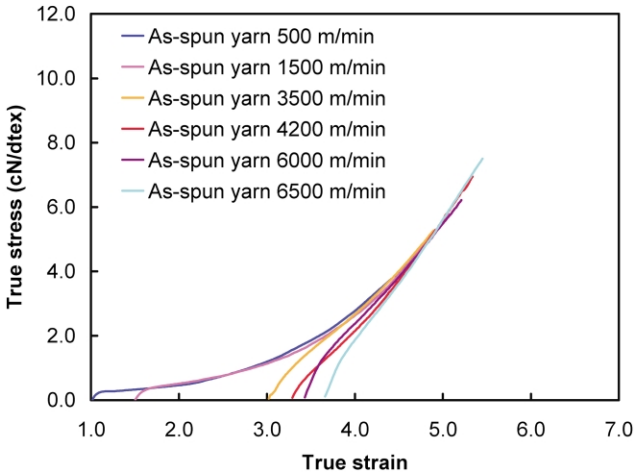

Fig. 3. Shifted true stress–strain curves for undrawn Nylon-6 yarns obtained at different wind-up speeds, as indicated in the legend.

change in network topology with increasing wind-up speed. Based on a detailed structural investigation of Nylon-6 yarns, Heuvel and Huisman [15] found that a transition in structure-formation mechanism occurs at wind-up speeds of about 3000 m/min, associated with the onset of spin line crystallization.

The shape of the mastercurve obtained by curve-matching provides information concerning the characteristics of the molecular network and may be interpreted in terms of rubber-elastic models. A detailed account on rubber-elastic modelling of the true stress–strain curves for Nylon-4,6 (Stanyl®) yarns is given in [7]. In a preliminary analysis of Nylon-6 yarns [16] it was found that the Edwards–Vilgis model [17] provides the best rubber-elastic description of the present true stress–strain data. Fig. 4 shows the experimental Nylon-6 mastercurve together with the Gaussian and Edwards–Vilgis fitted curves. The Edwards–Vilgis model yields a value of 8.0 for the maximum network draw ratio of Nylon-6 and describes

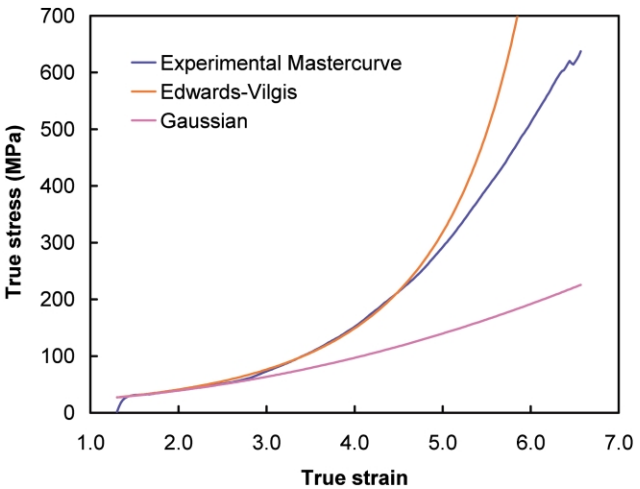

Fig. 4. Rubber-elastic modelling of the Nylon-6 mastercurve obtained by true stress–strain analysis. Application of the Gaussian and Edwards–Vilgis models.

the strain-hardening behaviour quite well up to network draw ratios of about 5.0. At higher network draw ratios, the observed strain-hardening behaviour falls short of the rubber-elastic prediction. This suggests topological changes in network structure when drawing to very high network draw ratios.

3.2. Orientation development

The network draw ratio reflects the state of deformation of the molecular network present in the undrawn and drawn Nylon-6 fibres. At this point, it is of interest to look at the development of molecular orientation with network draw ratio, since this provides insight into the mechanisms of deformation throughout fibre processing. Before doing so, let us first consider two theoretical schemes for prediction of orientation from network deformation: the *affine* and *pseudo-affine* deformation mechanisms [18]. In the affine scheme, network junctions are thought to be connected by flexible chains. Upon stretching, the network points are displaced in direct proportion to the macroscopic deformation. As a result, the rotatable 'random links' comprising the network chains will gradually adopt a more and more oriented configuration. For this type of rubber-like deformation, the orientation parameter $\langle P_2 \rangle$ can be described as a function of the network draw ratio λ according to

$$\langle P_2 \rangle = \frac{\Delta n}{\Delta n_{\max}} = \frac{1}{5N}\left(\lambda^2 - \frac{1}{\lambda}\right) \quad (4)$$

where Δn is the sample birefringence, $\Delta n_{\max}$ is the intrinsic birefringence and N is the number of random links between network points.

In pseudo-affine deformation, on the other hand, the structural elements undergoing deformation are assumed to have no extensibility themselves but are rigid entities simply rotating in proportion to the macroscopic deformation of the sample. This leads to [18]:

$$\langle P_2 \rangle = \frac{\Delta n}{\Delta n_{\max}} = \frac{1}{2}\left(\frac{2\lambda^3 + 1}{\lambda^3 - 1} - \frac{3\lambda^3}{(\lambda^3 - 1)^{3/2}}\arctan(\lambda^3 - 1)^{1/2}\right) \quad (5)$$

Fig. 5 shows the birefringence of an extensive set of Nylon-6 fibres, comprising LOY, POY and FDY, as a function of the network draw ratio determined by true stress–strain curve analysis described in the previous section. Fig. 5 also shows the development of orientation calculated for the affine and pseudo-affine deformation models using Eqs. (4) and (5). The calculations are made using $\Delta n_{\max} = 0.078$, a value obtained from literature data [9].

It is quite obvious from Fig. 5 that orientation development in Nylon-6 fibres follows a pseudo-affine deformation mechanism. It is surprising to find that the experimental data fit so well with theoretical prediction, given the fact that the pseudo-affine model has no fitting parameters, and that a set of samples with widely differing processing history is compared on the basis of a single parameter, the network draw ratio. The result seems to confirm the applicability of a network deformation model to Nylon-6. However, it may be noted that the undrawn POY do not fit with the overall scheme equally well as LOY and FDY. This again raises the question whether the network topology is preserved at high wind-up speeds.

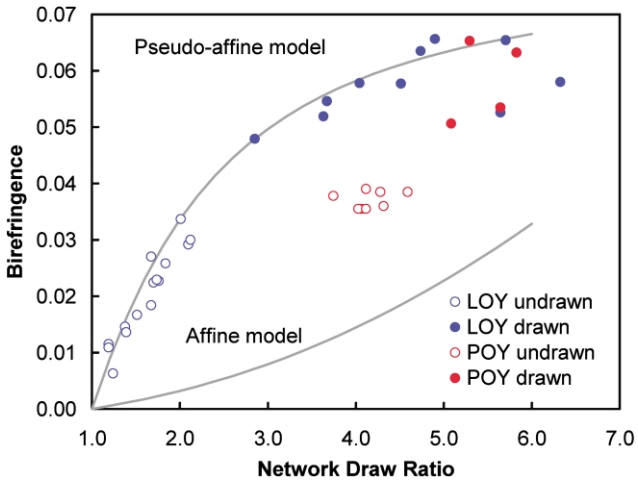

Fig. 5. Birefringence (after winding and conditioning) of different Nylon-6 yarns as a function of their network draw ratio, obtained by matching of true stress–strain curves. Theoretical predictions for affine and pseudo-affine models based on Eqs. (4) and (5) are also shown.

3.3. Structure development

The observation of pseudo-affine rather than affine deformation for melt-spun Nylon-6 fibres is, in itself, quite surprising. The early work of Ward and co-workers [1,2] has shown that orientation development in spun PET fibres follows the affine deformation theory of rubber elasticity. This is confirmed by various studies on melt spinning of PET [3–6,19] fibres, in which the development of birefringence with wind-up speed or network draw ratio is found to correspond to affine deformation behaviour as depicted by the lower curve in Fig. 5. We believe that the difference between Nylon-6 and PET in this respect can be attributed to differences in crystallization behaviour of the two polymers. Nylon-6 has a lower T_g than PET and the T_g of Nylon-6 shows a pronounced dependence on moisture content. As a result, Nylon-6 fibres tend to rapidly crystallize after winding and conditioning, even if crystallization does not occur in the spinning thread itself [15]. This means that undrawn Nylon-6 yarns are always partially crystalline, irrespective of wind-up speed. In contrast, undrawn PET yarns produced at low speed are fully amorphous but develop moderate levels of crystallinity at wind-up speeds sufficiently high to induce spin line

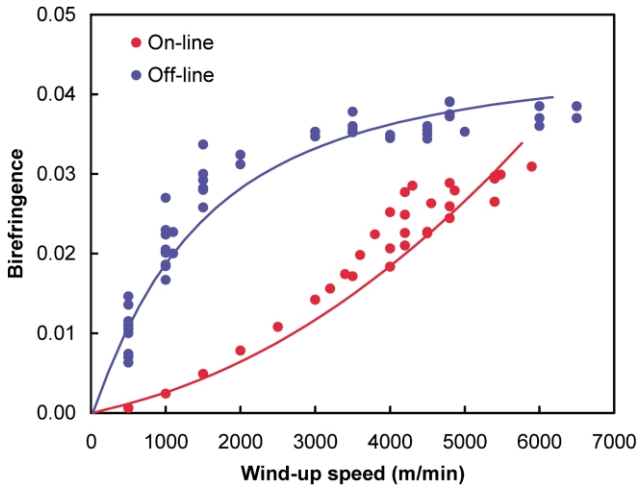

Fig. 6. Birefringence of Nylon-6 yarns as a function of wind-up speed, measured on the spinning thread ('on-line'), and after winding and conditioning ('off-line') of the spun yarns.

crystallization. It is reasonable to assume that the 'post-crystallization' behaviour of Nylon-6 plays an important role in the interpretation of orientation vs. deformation data.

In order to shed more light on crystallization phenomena during melt spinning of Nylon-6, we have studied the orientation development in the spin line by means of on-line birefringence measurement, as described in Section 2. Fig. 6 shows on-line birefringence and 'off-line' birefringence (measured after winding and conditioning), as a function of wind-up speed. A striking difference between the birefringence measured on-line and measured after winding and conditioning is observed. Comparing Figs. 5 and 6, it appears that the orientation behaviour of Nylon-6 in the spin line follows an affine deformation mechanism similar to melt spinning of PET. After winding and conditioning, the birefringence of the spun yarns changes dramatically, an effect associated with post-crystallization.

Qualitatively, an increase in birefringence upon crystallization suggests that the orientation factor of the developing crystalline phase is high, assuming that the orientation factor of the amorphous phase is not affected by the crystallization process. In a more quantitative approach, we may express the birefringence of a semicrystalline fibre in terms of crystallinity (V_c), crystalline and amorphous orientation factors (f_c and f_a) and intrinsic birefringence of the crystalline and amorphous phase ($\Delta n_{max,c}$ and $\Delta n_{max,a}$), according to Ref. [12]:

$$\Delta n = V_c f_c \Delta n_{max,c} + (1 - V_c) f_a \Delta n_{max,a} \quad (6)$$

For Nylon-6, we have $\Delta n_{max,c} = 0.089$ and $\Delta n_{max,a} = 0.078$ [9]. Since these values do not differ too much, a pronounced increase in birefringence upon crystallization can only occur if $f_c \gg f_a$.

In order to obtain a direct measure of crystalline and amorphous orientation in Nylon-6 fibres, a full characterization of fibre morphology has been made for a selected number of fibres from this study, using WAXS and solid-state NMR as described in Section 2. Since the characterization is made off-line, the structure data represent the morphology of the fibre after conditioning and crystallization. In addition to the off-line characterization techniques, a value for the amorphous orientation factor in the spinning fibre has been obtained from on-line birefringence measurements. Assuming that no crystallization occurs in the spinning line ($V_c = 0$), Eq. (6) reduces to $f_a = \Delta n / \Delta n_{max,a} = \Delta n / 0.078$. Thus, the amorphous orientation factor in the spinning fibre can be obtained directly from on-line birefringence.

Table 1 shows a selection of structure data for undrawn Nylon-6 fibres spun at different wind-up speeds. The level of crystallinity is seen to vary little with wind-up speed, going from 50% in undrawn LOY to 63% in undrawn POY, even though the mechanism of formation of the crystalline phase is completely different in LOY and POY yarns. The different mechanism of crystallization is however reflected in the composition of the crystalline phase, which consist of a mixture of α- and γ-crystals in LOY but contains predominantly γ-crystals at the highest winding speed.

Fig. 7 shows the amorphous and crystalline orientation factors of undrawn yarns as a function of wind-up speed. It is seen that f_c is already quite high at moderate wind-up speed, whereas f_a (both from solid-state NMR and on-line birefringence) develops slowly with wind-up speed. This result confirms the idea that the pronounced difference between on-line and off-line birefringence arises from post-crystallization, during which crystals with a relatively high orientation are formed ($f_c \gg f_a$).

It is quite surprising to find that a highly oriented crystalline phase develops in the spun yarns from a low oriented amorphous network structure. A similar behaviour has been observed in a recent study on drawing of PET films using real time WAXS measurements [20]. It was found that the very first crystals that are formed in the course of hot-drawing are already highly oriented ($f_c \approx 0.8$) and crystalline orientation appears to have no relation with the orientation state of the amorphous phase. Based on these results it was concluded that the crystalline phase starts to develop from highly oriented chain segments. Such chain

Table 1
Structure data for undrawn Nylon-6 fibres spun at various wind-up speeds (WUS)

WUS (m/min)	V_α (vol%)	V_γ (vol%)	$V_{c,tot}$ (vol%)	f_c		f_a	
				WAXS	NMR	NMR	On-line Δn
500	29	20	49	0.29	0.26	0.06	0.01
1100	30	21	51	0.56	0.57	0.19	0.03
3500	19	40	59	0.80	0.73	0.24	0.19
6000	16	46	63	0.69	0.79	0.47	0.45

V_α and V_γ represent the volume fractions of the α- and γ-crystalline phase and $V_{c,tot}$ is the overall crystallinity. f_c and f_a are the amorphous and crystalline orientation factors, obtained by different techniques as indicated.

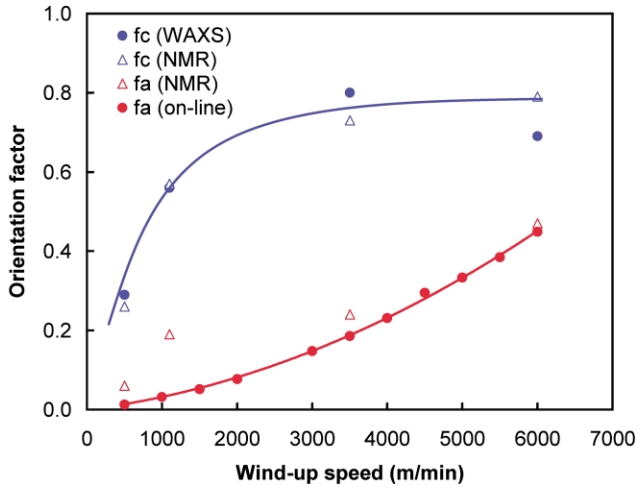

Fig. 7. Crystalline and amorphous orientation factors f_c and f_a of undrawn yarns as a function of wind-up speed determined from WAXS, solid-state NMR and on-line birefringence measurement.

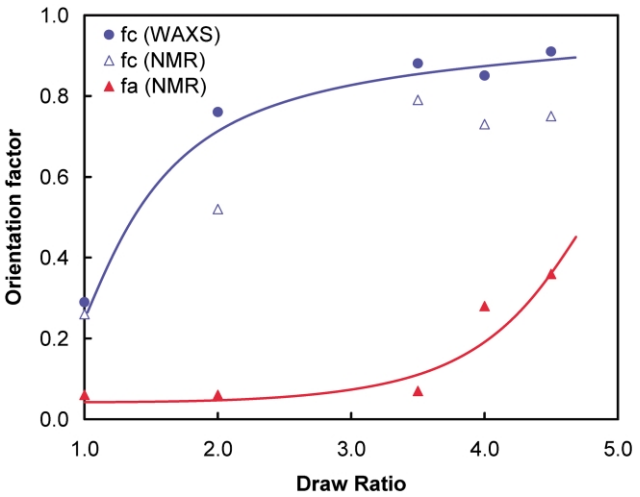

Fig. 8. Crystalline and amorphous orientation factors f_c and f_a of drawn yarns as a function of draw ratio determined from WAXS and solid-state NMR measurements.

segments may be short network chains that become fully extended already at low overall deformation of the network structure.

Fig. 7 also shows that there is a good agreement between amorphous orientation factors determined from on-line birefringence and NMR measurements. This result indicates that the amorphous network structure developed in the spinning thread is preserved in the fibre structure in spite of post-crystallization.

A further insight into the different orientation behaviour of the amorphous and crystalline phases in Nylon-6 is obtained from structure analysis on drawn yarns. Table 2 shows a selection of structure data for drawn yarns at various draw ratios, obtained from a 500 m/min LOY precursor. The amorphous and crystalline orientation factors are plotted as a function of draw ratio in Fig. 8. The orientation behaviour of the crystalline and amorphous phases is similar to that observed in Fig. 7. The crystalline orientation factor f_c initially increases sharply, levelling off at higher draw ratio whereas f_a initially rises very slowly becoming important only at the highest draw ratios. Comparing to Fig. 5, it appears that the crystalline phase responds to draw ratio in a pseudo-affine fashion whereas the amorphous phase follows a rubber-like, affine deformation. This result can be understood in qualitative terms since crystallites act as rigid entities in the fibre structure whereas the amorphous phase consists of flexible chains, acting as a rubber network. Since the amorphous orientation is comparatively low at the maximum draw ratios, it is reasonable to assume that further drawing is hampered by the crystalline phase.

Table 2
Selected structural data for Nylon-6 fibres spun at 500 m/min and drawn to different draw ratios (DR)

DR	V_α (vol%)	V_γ (vol%)	$V_{c,tot}$ (vol%)	f_c		f_a
				WAXS	NMR	NMR
–	29	20	49	0.29	0.26	0.06
2.0	39	11	50	0.76	0.52	0.06
3.5	49	5	54	0.88	0.79	0.07
4.0	42	2	44	0.85	0.73	0.28
4.5	57	0	57	0.91	0.75	0.36

Finally, it should be noted that the overall birefringence is dominated by the crystalline phase. Combining structure data with equation 6, it turns out that, in the as-spun yarns, the crystalline phase contributes about 75–85% to the overall birefringence, irrespective of wind-up speed. For drawn yarns, this effect is even more pronounced and the crystalline phase contributes about 85–95% to the overall birefringence at all draw ratios. A similar behaviour was observed for polyethylene, where the birefringence of the crystalline phase accounts for about two-thirds of the total [12]. Thus, the *overall* orientation appears to vary with network draw ratio (Fig. 5) or wind-up speed (Fig. 6) much in the same way as does the crystalline orientation, in a predominantly pseudo-affine fashion. This is in remarkable contrast with the fact that the mechanical response to deformation is described so well by the Edwards–Vilgis model with its underlying physics of affine, rubber-like network elements. A possible explanation is that the mechanical response to deformation is dominated by the underlying amorphous network in the fibre structure, in which crystallites may act as network junctions but do not contribute significantly to the generation of stress. This would explain why the amorphous network dominates the mechanical response, whereas the crystalline phase dominates the optical response of the fibre.

4. Conclusions

From the results of this study, it is evident that the

network model provides a very useful approach in understanding orientation and structure development in Nylon-6 fibres. The network draw ratio can be conveniently obtained by superposition of true stress–strain curves and can be correlated with fibre orientation using well-known relationships for network deformation. The approach works particularly well for fibres produced at low winding speeds and drawn to moderate draw ratios. However, the network does not appear to retain its original structure under processing conditions that lead to high orientation, such as high winding speeds or draw ratios close to the maximum value.

The analysis of structure data emphasizes the importance of the semicrystalline nature of Nylon-6 fibres with respect to deformation and orientation behaviour. Based on the present data, a consistent picture of orientation and structure development in Nylon-6 fibres emerges. In the spinning thread, in the absence of crystallinity, the polymer behaves as a single phase rubber-like network, adhering to affine deformation similar to spinning of PET. Due to a post-crystallization process that occurs after winding and conditioning, Nylon-6 fibres develop a substantial level of crystallinity (50% or more) even at low wind-up speeds. The structure of the amorphous network developed in the spinning thread is preserved in the final wound sample in spite of post-crystallization. The orientation of the crystalline phase that develops during post-crystallization is relatively high already at low wind-up speed. Apparently, post-crystallization starts from highly oriented amorphous segments, such as short network chains that become fully extended at low overall network deformation. Post-crystallization leads to a pronounced difference in birefringence determined on-line and after winding. In subsequent hot-drawing of the semicrystalline spun yarns, the crystalline phase deforms according to a pseudo-affine mechanism where the crystallites act as rigid structural entities. The amorphous phase, on the other hand, retains its rubber-like behaviour and deforms according to an affine mechanism. As a result, the development of orientation with network draw ratio is entirely different for the two phases present in the fibre structure. An important consequence is that the orientation of the crystalline phase is always much higher than that of the amorphous phase, implying that the drawability of Nylon-6 fibres is limited by the crystalline phase. Another consequence is that the crystalline phase contributes more than 75% to the overall birefringence, irrespective of wind-up speed or draw ratio. As a result, the overall orientation varies with network draw ratio much in the same way as crystalline orientation does, that is, in pseudo-affine fashion. This appears to be in contrast with the fact that the mechanical response of the fibre is described so well by the Edwards–Vilgis model, which is based on affine, rubber-like network deformation. A possible explanation is that the crystallites in the fibre structure act as network junctions but do not contribute significantly to stress, meaning that the amorphous network dominates the mechanical response, whereas the crystalline phase dominates the optical response of the fibre.

Acknowledgements

Professor Ian Ward is gratefully acknowledged for many helpful and stimulating discussions on the subject of network deformation in polymeric fibres. The authors also wish to acknowledge Dr Rudy Deblieck (DSM Research) for support on rubber-elastic modelling of Nylon-6 fibres. Dr Harry Feijen and Ir. Kees Bos (Acordis Industrial Fibres, Arnhem, The Netherlands) are acknowledged for making available the on-line birefringence measurement device.

References

[1] Pinnock PR, Ward IM. Trans Faraday Soc 1966;62:1308–20.
[2] Allison SW, Pinnock PR, Ward IM. Polymer 1966;7:66–9.
[3] Brody HJ. Macromol Sci Phys 1983;B22:19–41.
[4] Long SD, Ward IM. J Appl Polym Sci 1991;42:1911–20.
[5] Cansfield DLM, Patel R, Ward IM. J Macromol Sci Phys 1993;B32:373–93.
[6] Shirataki H, Nakashima A, Sato K, Okajima K. J Appl Polym Sci 1997;64:2631–46.
[7] Van Ruiten J, Riedel R, Deblieck R, Brouwer R, Penning JP. J Mater Sci 2001;36:3119–28.
[8] Schreiber R, Veeman WS, Gabriëlse W, Arnauts J. Macromolecules 1999;32:4647–57.
[9] Balcerzyk E, Kozlowski W, Wesolowska E, Lewaszkiewicz WJ. Appl Polym Sci 1981;26:2573–80.
[10] Van Krevelen DW. Properties of polymers, 3rd ed. Amsterdam: Elsevier; 1990.
[11] Salem DR, Moore RAF, Weigmann HD. J Polym Sci, Polym Phys Ed 1987;25:567–89.
[12] Stein RS, Norris FH. J Polym Sci 1956;21:381–96.
[13] Harris PH. UK Patent Application GB2,049,175; 1980
[14] Nagasawa M, Koizuka A, Matsuura K, Horita M. Macromolecules 1990;23:5079–82.
[15] Heuvel HM, Huisman RJ. Appl Polym Sci 1981;26:713–32.
[16] Deblieck R. DSM Research. Private communication
[17] Edwards SF, Vilgis T. Polymer 1986;27:483–92.
[18] Ward IM. Structure and properties of oriented polymers, 2nd ed.; 1997. p. 37–41.
[19] Heuvel HM, Huisman R. J Appl Polym Sci 1978;22:2229–43.
[20] Middleton AC, Duckett RA, Ward IM, Mahendrasingam A, Martin CJ. Appl Polym Sci 2001;79:1825–37.